Lateral electron transport in thin foils diagnosed by ion emission

P. McKenna, D. C. Carroll, K. W. D. Ledingham*, T. McCanny and L. Robson*
SUPA, Department of Physics, University of Strathclyde, Glasgow, G4 0NG, UK

R. J. Clarke, R. G. Evans#, A. P. L. Robinson and D. Neely
Central Laser Facility, STFC, Rutherford Appleton Laboratory, Chilton, Didcot, Oxon, OX14 0QX, UK

F. Lindau, O. Lundh and C.-G. Wahlström
Department of Physics, Lund University, P. O. Box 118, S-22100 Lund, Sweden

P. T. Simpson and M. Zepf
Department of Physics and Astronomy, Queen's University Belfast, Belfast, BT7 1NN, UK

*also at AWE plc, Aldermaston, Reading, RG7 4PR, UK
also at Blackett Laboratory, Imperial College London, London, SW7 2AZ, UK

Main contact email address **p.mckenna@phys.strath.ac.uk**

Introduction

The study of fast electron transport in intense laser interactions with dense plasma is of fundamental importance for fast ignition[1,2], and for the optimization of high power laser-driven ion sources[3-5]. Experimental and theoretical investigations in the 1980s, at laser intensities up to ~10^{16} W/cm^2, revealed that ~30% of the absorbed laser energy is transported laterally by energetic electrons[6,7].

In this letter we present an experimental investigation of lateral electron transport in target foils irradiated at ultrahigh intensities, up to 6×10^{20} W/cm^2. We demonstrate the use of spatially resolved measurements of multi-MeV ion emission as a diagnostic of electric-field (E-field) generation resulting from electron transport. Ion emission has previously been used to investigate field dynamics at the rear of a target foil, opposite to the laser focal spot[8]. Here we observe and measure ion emission from the edges of thin target foils, where the edges are sufficiently far away from the focal spot that the expanding electron cloud cannot reach them until a long time after the laser pulse. We use this ion emission to make quantitative measurements of the 2D spatial distribution of E-field formation due to lateral electron transport in the foil. We also present simulation results using the implicit particle-in-cell (PIC) LSP code[9], which reveals enhanced electron densities and E-fields at solid-vacuum boundaries.

Experimental

The experiment used the Vulcan laser, delivering pulses of wavelength 1.053 μm, energy up to 400 J and duration 1 ps (FWHM). The ASE level is measured to be 10^{-7} and 10^{-6} of the peak laser intensity at a few nanoseconds and a few picoseconds prior to the peak of the pulse, respectively. The *p*-polarised pulses are incident onto target at 45º.

Ten micron thick planar Au and Al foils of size 4 mm × 10 mm are used as targets. Some of the foils had 50 μm diameter 'witness' holes machined 500 μm from the laser focus. The Au targets are resistively heated to 1000ºC for 10 minutes prior to and during laser irradiation, to reduce the hydrogenated contamination on the target surfaces. This results in more efficient acceleration of ions heavier than protons.

A high-resolution Thomson spectrometer is used to measure the charge-to-mass ratio and energy of ions emitted from the target. The spectrometer design involves a 0.6 T magnetic field and an electric field which varies in strength from 3.0 to 0.3 kV/mm over a distance of 200 mm. The spectrometer has been described in a previous CLF Annual Report[10]. The solid angle sampled by the spectrometer is between 5×10^{-9} and 2×10^{-7} Sr, depending on the ion flux. A CR-39 plastic track detector, positioned in the dispersion plane, is used to detect ions (and fast neutral atoms). The spatial distribution of the pits in the CR-39 is mapped out using an automated scanning microscope with pit recognition and analysis software[11].

Results

We find that, regardless of whether we irradiate Al or Au foils, heated or unheated, we observe ion emission from the edges of the target foils, 2 mm on either side of the laser focal spot. Figure 1, which shows part of an optically scanned image of pits produced in a CR-39 sample, illustrates the observation. The Thomson spectrometer in this example was positioned along the target normal axis at the rear of a 10 μm thick unheated Al target, irradiated by a 200 J, 1 ps, 3×10^{20} W/cm^2 laser pulse. The image is produced by fast neutral atoms, which result from fast ions undergoing recombination before entering the spectrometer. These fast neutral particles are detected on every shot and typically correspond to ~3% of the total ion signal detected on the CR-39. The pits produced by these recombined ions mark the zero-deflection axis of the spectrometer onto the CR-39 detector, and are useful for

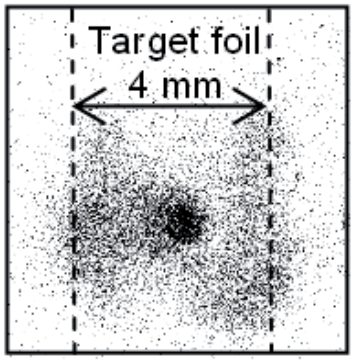

Figure 1. (a) Optical scanned image of pits in CR-39 produced by fast uncharged atoms (recombined ions). The CR-39 was positioned at the back of a Thomson spectrometer acting as a pinhole camera. Ions are accelerated from a central spot and from linear regions corresponding to the target edges.

calibrating the ion energy spectra. Figure 1 is in effect a 2-D spatially resolved measurement of ion emission. Most ions are emitted from a region opposite to the laser focal spot. Linear regions of ion emission on either side of the central spot are also observed, and correspond to ion emission from the edges of the target.

The measurement in figure 1 was made using a pinhole with diameter 300 μm at the entrance of the spectrometer. Next we decrease the pinhole size to 50 μm to increase the spatial resolution of the technique. Figure 2 shows a spatial mapping, at the higher resolution, of pits distributed in a full CR-39 detector. This measurement was made with a 340 J energy laser pulse focused to a spot size of 40 μm (FWHM), corresponding to an intensity of 1×10^{19} W/cm^2, onto a heated Au foil target. Mainly carbon ions are observed, from hydrocarbon contamination layers. Two main features of interest in the figure are enlarged. As with the measurement in figure 1, we observe ion emission from the edges of the target (C and D). The signal is considerably reduced due to a factor of 36 reduction in the solid angle sampled by the spectrometer and a factor 30 reduction in laser intensity. An additional ion source (B), vertically offset from the main source (A), corresponds to emission from the edge of a 50 μm diameter 'witness' hole positioned 500 μm from the focal spot. With the higher spatial resolution we observe multiple ion tracks for many of the charge states of carbon, as shown in an inset of figure 2. Each track has been identified as resulting from one of the four ion sources, revealing that, in addition to the main source (A) carbon ions are also emitted from the edges of the irradiated target foil and the hole. The ions emitted from each source are listed in Table 1.

Using the method described by Hegelich *et al.* [8], we use carbon ion emission to diagnose E-field generation. The charge states provide a measure of the peak E-field strength and the maximum ion energy provides information on the temporal and spatial extent of the field. Similar to Hegelich *et al* [8] we calculate that the collisional ionization rate due to the hot electrons and the cold electron return current is lower than the ionization

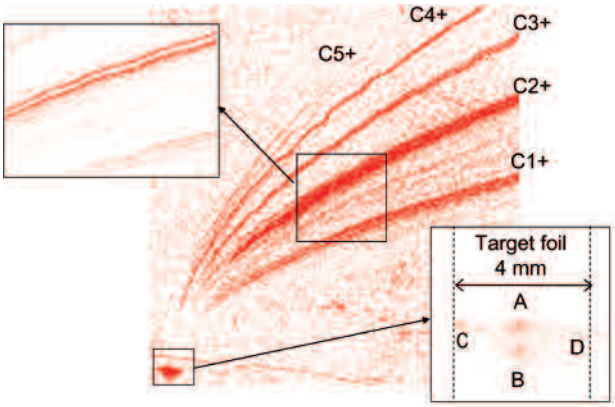

Figure 2. Spatial mapping of pit distributions on a CR-39 detector in the dispersion plane of a Thomson spectrometer. Carbon ions are detected in distinct ion traces. Multiple tracks are observed for some of the ion species, as shown in the top inset. The tracks are produced from four source regions on the target, corresponding to the centre of the target foil, A, at the edge of a 50 μm hole, B, and at the edges of the foil, C and D, as shown in the bottom inset.

	q	$E_q^{Thres.}$ (TV/m)	$E_q^{max.}$ (TV/m)	$\tau_q^{min.}$ (ps)	$l_q^{min.}$ (μm)
A	1	0.022	0.052	18	69
	2	0.052	0.13	4.4	21
	3	0.13	0.18	3.1	22
	4	0.18	5.3	0.12	1.2
	5	5.3	7.0	0.09	1.1
B	1	0.022	0.052	21	95
	2	0.052	0.13	4.6	23
	3	0.13	0.18	4.0	36
C	1	0.022	0.052	11.7	29
	2	0.052	0.13	4.0	17
D	2	0.052	0.13	…	…

Table 1. C^{q+} ions observed from each of the four sources (A to D) in figure 2 and calculated field parameters. $E_q^{Thres.}$ is the lower threshold E-field required to produce a carbon ion of charge q. E_q^{max} is the maximum E-field and is used to calculate τ_q^{min} and l_q^{min}, the minimum field duration and acceleration length to accelerate the ionic charge state to the detected maximum energy.

rate due to Field Ionization by Barrier Suppression (FIBS) for C^{q+}: q=1 to 4, and thereby assume FIBS to be the dominant ionization mechanism at the rear of the target. The threshold field $E_q^{Thres.}$ for the production of each ion of charge q is calculated using:

$$E_q^{Thres.} = U_{q-1}^2 \varepsilon_0 \pi / q.e$$

where U_q is the ionization potential in eV. A lower limit for the acceleration time τ and the acceleration length l (minimum longitudinal spatial extent of the field) required to produce the measured maximum energy of each ion species from each source is calculated assuming that a given ion of charge q will experience a maximum electric field strength given by $E_q^{max} = E_{q+1}^{Thres.}$, the threshold for further ionization. The calculated parameters for each of the four sources are presented in Table 1.

The highest field strength, >5.3 TV/m, is produced in the region of the target rear surface opposite to the laser focal spot. The strength of the field generated on the edge of the hole 0.5 mm from the focal spot is between 0.13 and 0.18 TV/m and fields of between 0.05 and 0.13 TV/m are generated at the edges of the target. E-fields of this order 2 mm away from the focal spot, indicates that the lateral transport of energetic electrons in the foil continues long after the laser pulse. This is consistent with time resolved measurements of K_α X-ray production for thin, isolated targets [12].

Simulations

We perform 2D cylindrical simulations of the charge cloud dynamics with the LSP computer model [9]. A kinetic (PIC) description of the energetic electrons and a fluid description of the bulk of the target are used. The simulation grid consists of 2400 × 2400 cells covering an area 600 μm by 600 μm. The cell size of 0.25 μm is adequate to resolve the distribution of electrons in the

bulk of the 10 μm thick target foils, but does not enable investigation of ion dynamics. Electrons are created to correspond to the distribution of accelerated electrons from the laser. A laser-to-electron energy conversion efficiency of 30% is assumed and the mean electron energy is 1 MeV, equal to the ponderomotive potential, for a laser intensity of 10^{19} W/cm^2.

For a laser pulse of duration T the electron temperature is increased over 0.1T, held constant for 0.8T and decreased over 0.1T. The axial distribution corresponds to half of a relativistic thermal distribution (in the laser direction) and the angular spread is around 30 degrees half angle. Many of the electrons which pass through the target are reflected in the expanding Debye sheath on the rear surface. As the electrons reflux[13] many times within the foil, the charge cloud expands out laterally forming a disk, due to the transverse component of the electron velocity. The radial expansion requires a return current to flow via the 'cold' electrons of the target foil and the resistivity of the target gives rise to an E-field which hinders the expansion. Due to the fall off in current density as the cloud expands radially the effect of this E-field rapidly diminishes with radius.

The LSP simulations show a very strong enhancement of the electron density and E-field when the charge cloud reaches the edge of the target. This is illustrated in the results of figure 3, which shows the hot electron density and magnitude of the resulting E-field 2.5 ps after the start of the laser pulse. The return current is no longer supported at the edge of the target and the expansion is halted by the radial component of the electrostatic field caused by the build up of net negative charge. The electrons 'pile-up' at the target edge and are eventually reflected after a time of order of the plasma period (300 fs for an electron density of 10^{17} cm^{-3}). The E-fields at the target edge in the simulation (400 μm radius) are about 0.2 TV/m and fields greater than 0.02 TV/m extend out to a distance of about 15 μm from the target.

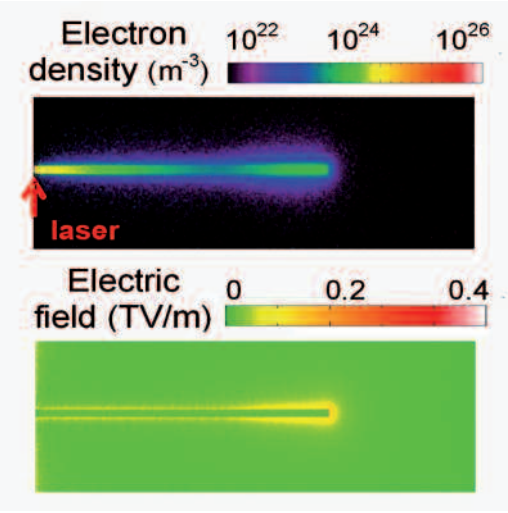

Figure 3. LSP simulation result showing electron density and resultant E-field strength 2.5 ps after the start of the laser pulse. The target has a radius equal to 400 μm and thickness equal to 10 μm. The simulation space is cylindrically symmetric about the laser axis, marked by the red arrow.

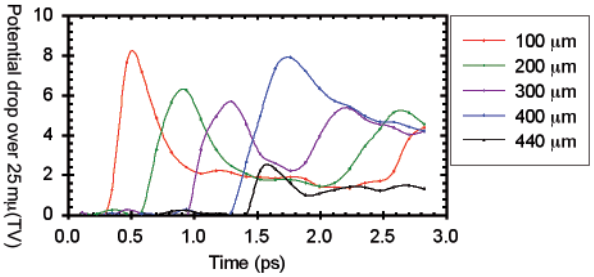

Figure 4. Temporal evolution of the potential drop over 25 μm from the surface of the target at given radii from the laser focal spot. The field becomes higher and remains high at the edge of the target (400 μm) for much longer than at smaller radii.

Figure 4 shows the temporal evolution of the E-field (potential drop over a distance of 25 μm from the surface of the target in the direction normal to the surface) as a function of time for selected distances from the laser focal spot. The radius of the target in the simulation is 400 μm and in the experiment is 2 mm, and therefore a pulse duration of 200 fs is used in the simulation - scaled down to the transit time for the expanding charge cloud to reach the target edge. It is observed that the charge wave moves laterally at approximately 0.75c. The magnitude of the field at the edge remains large over a much longer duration than the transient field at other radii within the target. Ion emission as a diagnostic of E-field generation is more sensitive to the longer duration field at the edges. Ion emission therefore provides a unique probe of transient E-field strength in intense laser-foil interactions.

Summary

We have shown that there is significant lateral expansion of the electron cloud in thin foils irradiated by ultraintense laser pulses and that the electron motion is inhibited at target-vacuum interfaces, leading to the formation of strong electric fields and resulting in ionization and ion acceleration. Using ion emission to quantify the E-field at varying distances from the laser focus, we have also shown that hot electron transport occurs long after the time of the laser pulse driver.

This work has been published in reference[14], and we plan to investigate the lateral dynamics of fast electrons in more detail in future experiments.

The authors would like to acknowledge the Vulcan staff. OL and FL acknowledge support from the COST Action.

References

1. M. Tabak *et al.*, *Physics of Plasmas* **1**, 1626 (1994).
2. R. Kodama *et al.*, *Nature* **412**, 798 (2001).
3. M. Borghesi *et al.*, *Fusion Science and Technology* **49**, 412 (2006).
4. K. W. D. Ledingham, P. McKenna, and R. P. Singhal, *Science* **300**, 1107 (2003).
5. M. Roth *et al.*, *Physical Review Special Topics-Accelerators and Beams* **5**, 061301 (2002).
6. D. W. Forslund and J. U. Brackbill, *Physical Review Letters* **48**, 1614 (1982).
7. F. Amiranoff *et al.*, *Journal of Physics D: Applied Physics* **15**, 2463 (1982).

8. M. Hegelich *et al*., *Physical Review Letters* **89**, 085002 (2002).
9. D. R. Welch *et al*., *Nuclear Instruments and Methods in Physics Research A* **464**, 134 (2001).
10. D. Carroll *et al*., Central Laser Facility, Rutherford Appleton Laboratory Annual Report 2005-06 **26**.
11. TASL-IMAGE, Track Analysis Systems Limited; Details online at www.tasl.co.uk (2006).
12. J. C. Kieffer *et al*., *Journal of the Optical Society of America B* **13**, 132 (1996).
13. Y. Sentoku *et al*., *Physics of Plasmas* **10**, 2009 (2003).
14. P. McKenna *et al*., *Physical Review Letters* **98**, 145001 (2007).